Biosensors and Bioelectronics: X 27 (2025) 100687

Contents lists available at ScienceDirect

Biosensors and Bioelectronics: X

journal homepage: www.journals.elsevier.com/biosensors-and-bioelectronics-x

Paper-based origami assisted and enhanced electroanalytical detection of β-Amyloid peptide in plasma samples

Antonella Miglione [a,*], Panagiota M. Kalligosfyri [a], Claudia Corbo [b,c], Donato Calabria [d], Mara Mirasoli [d], Marco Frasconi [e], Stefano Cinti [a,f,g,**]

[a] Department of Pharmacy, University of Naples "Federico II", 80131, Naples, Italy
[b] School of Medicine and Surgery, Nanomedicine Center Nanomib, University of Milano-Bicocca, Via R. Follereau 3, Vedano al Lambro, MB, 20854, Italy
[c] IRCCS Istituto Ortopedico Galeazzi, Via Cristina Belgioioso 173, Milan, 20161, Italy
[d] Department of Chemistry "G. Ciamician", University of Bologna, 40126, Bologna, Italy
[e] Department of Chemical Sciences, University of Padova, Via Marzolo 1, Padova, 35131, Italy
[f] Sbarro Institute for Cancer Research and Molecular Medicine, Center for Biotechnology, College of Science and Technology, Temple University, Philadelphia, PA, 19122, USA
[g] Bioelectronics Task Force at University of Naples Federico II, Via Cinthia 21, Naples, 80126, Italy

ARTICLE INFO

Keywords:
Alzheimer's disease
β-amyloid
Screen-printed electrodes
Paper-based
Point-of-care

ABSTRACT

In this work, we demonstrate how the analytical performance towards β-amyloid (Aβ(1–42) detection can be easily improved by using a printed label-free electrochemical immunosensor coupled to an external paper-based origami. Coupling the immunosensor with a customized foldable origami allows for an increase of resulting sensitivity towards the detection of Aβ(1–42) in both standard and biological samples. The features of paper are fundamental for the analysis of Aβ(1–42), recognized as a central indicator of Alzheimer's pathology, considering the low levels in plasma associated with early-stage disease. The proposed strategy highlights up to a 5-fold signal enhancement in both buffer and plasma at low Aβ(1–42) concentrations, bringing the platform's performance toward clinical requirements. The immunoplatform has been systematically optimized through electrochemical characterization and parameter tuning, achieving limits of detection of 2.7 ng/mL in buffer and 4.7 ng/mL in undiluted plasma, with a linear range up to 1 μg/mL. The platform shows satisfactory repeatability (<10 %) and excellent selectivity in the presence of interfering plasma proteins. Overall, this work offers a promising foundation for the development of accessible and scalable tools for early Alzheimer's disease screening.

1. Introduction

Alzheimer's disease (AD) is the most prevalent neurodegenerative disorder, accounting for 60–70 % of dementia cases worldwide and affecting over 55 million people (Knopman et al., 2021; Safiri et al., 2024). As populations age, the incidence of dementia is projected to rise dramatically in the coming decades, placing increasing pressure on healthcare systems and caregivers. Given the disease's irreversible progression and lack of a definitive cure, early and accurate diagnosis is critical to enable timely intervention (Mei et al., 2024; Safiri et al., 2024; Zhang et al., 2024). One of the earliest and most well-established pathological hallmarks of AD is the accumulation of β-amyloid peptides, particularly Aβ(1–42), which form extracellular plaques in the brain (Azargoonjahromi, 2024; Karapetyan et al., 2022). These peptides are derived from the proteolytic cleavage of amyloid precursor protein (APP), and they are recognized as core biomarkers for early and accurate diagnosis (Karran and De Strooper, 2022; Seppälä et al., 2010).

While cerebrospinal fluid (CSF) remains the gold standard matrix for measuring Aβ levels, its collection is invasive and unsuitable for population-level screening or longitudinal monitoring (Bouwman et al., 2022). Current Aβ detection techniques include enzyme-linked immunosorbent assays (ELISA) (Bun et al., 2023), mass spectrometry (MS) (Kirmess et al., 2021; Korecka and Shaw, 2021), and positron emission tomography (PET) (Minoshima et al., 2016; Suppiah et al., 2019). While

This article is part of a special issue entitled: Smart Biosensors published in Biosensors and Bioelectronics: X.

* Corresponding author.
** Corresponding author. Department of Pharmacy, University of Naples "Federico II", 80131, Naples, Italy.
E-mail addresses: antonella.miglione@unina.it (A. Miglione), stefano.cinti@unina.it (S. Cinti).

https://doi.org/10.1016/j.biosx.2025.100687
Received 19 July 2025; Received in revised form 30 August 2025; Accepted 17 September 2025
Available online 23 September 2025

ELISA and MS offer high sensitivity and specificity, they are time-consuming, expensive, and require centralized laboratories with skilled personnel (Bun et al., 2023; Kirmess et al., 2021; Weber et al., 2024). PET imaging, though effective for visualizing amyloid deposition *in vivo*, involves radioactive tracers and is not suitable for routine screening or early-stage monitoring (Suppiah et al., 2019). These limitations highlight the urgent need for accessible, rapid, and cost-effective diagnostic tools. As a result, there is growing clinical and research interest in developing blood-based diagnostic tools for minimally invasive and more accessible detection of Aβ peptides (Delaby et al., 2023; Schindler et al., 2024). However, detecting Aβ(1–42) in plasma is particularly challenging, due to its extremely low abundance (Janelidze et al., 2016). In cognitively healthy individuals, plasma concentrations of Aβ(1–42) typically range from 8 to 30 pg/mL (Zecca et al., 2018), with levels potentially rising to 30–50 pg/mL in preclinical stages of AD, before decreasing again, often below 20 pg/mL, in mild cognitive impairment (MCI) and AD (Chen et al., 2019; Lue et al., 2017). As a result, only highly sensitive and selective technologies can meet the analytical demands of plasma-based Aβ detection. In fact, the first blood-based diagnostic aid for Alzheimer's was only recently authorized (May 2025) by the U.S. Food and Drug Administration (FDA): it consists in a chemiluminescent immunoassay, named Lumipulse® G pTau217/β-Amyloid 1–42 Plasma Ratio, that is able to quantify both phosphorylated tau and Aβ(1–42) in plasma, using their ratio as a surrogate marker of amyloid pathology (FDA, 2025). Although the test offers high sensitivity, reportedly detecting Aβ in the 1–2 pg/mL range, it still relies on centralized laboratory instrumentation and skilled personnel, limiting its scalability and utility for decentralized or point-of-care (PoC) applications (Bellomo et al., 2024). Electrochemical biosensors, on the other hand, have shown strong potential for bridging this gap, offering low-cost fabrication, fast response times, and miniaturization compatibility (Chiorcea-Paquim and Oliveira-Brett, 2022; Ding et al., 2023; Hassan and Kerman, 2019; Sharma et al., 2023; Valkova and Pohanka, 2021). In particular, screen-printed electrodes (SPEs) have been widely explored for AD biomarkers, thanks to their ease of production and potential for integration into portable formats (Rama et al., 2014; Sethi et al., 2020; Singh et al., 2022; Y. Abbasi et al., 2021). However, many of these rely on label-based detection strategies involving enzymatic or fluorescent tags, which can complicate fabrication, reduce stability, and hinder real-time or field applications (Rama et al., 2014; Wang et al., 2022). Label-based electrochemical immunoassays for Aβ(1–42) have demonstrated detection limits near 0.1 ng/mL (Rama et al., 2014), with recent innovations, including disposable SPE sensors, achieving as low as 1 pg/mL over narrow dynamic ranges (Li et al., 2023). Other advanced platforms, such as paper-based superwettable gold chips, have reached 0.012 pg/mL LOD in serum, though they rely on complex nanofabrication (Huang et al., 2022). Notably, fully label-free, low-cost electrochemical sensors at clinically relevant sensitivities remain rare (Carneiro et al., 2017; Sethi et al., 2020; Y. Abbasi et al., 2021).

Here, we present a label-free electrochemical immunosensor for the detection of Aβ(1–42), based on screen-printed electrodes (SPEs) and enhanced by a preconcentration method, aimed at closing the sensitivity gap. This preconcentration device is based on a paper-based origami architecture previously developed and validated by our group for the enrichment of a variety of biomolecules, including miRNAs, dsDNA, and small molecules, demonstrating its versatility, speed, and compatibility with low-resource diagnostic formats (Cimmino et al., 2024; Glovi et al., 2025; Kalligosfyri and Cinti, 2024; Raucci et al., 2025). Most importantly, origami preconcentration achieved a 4–5x enhancement in current signal at low analyte concentrations, marking a significant step toward clinically relevant detection. This work demonstrates that the use of a paper-based preconcentration strategy can effectively substitute for conventional signal amplification tags, enabling enhanced sensitivity without added complexity. Consequently, it provides a promising foundation for the future development of affordable, accessible, and portable screening tools for early Alzheimer's diagnosis, especially in resource-limited settings.

2. Experimental section

2.1. Reagents and solutions

Anti-beta Amyloid antibody [DE2B4] (ab11132) (anti-Aβ(1–42)) and beta-Amyloid Peptide (Aβ(1–42)) (human) (ab120301) were purchased from Abcam (Cambridge, UK). Gold (III) chloride trihydrate ($HAuCl_4 \cdot 3H_2O$), 3-Mercaptopropionic acid (MPA), 1-Ethyl-3-(3-dimethylaminopropyl) carbodiimide hydrochloride (EDC HCl), *N*-Hydroxysuccinimide (NHS), Tween® 20, Bovine serum albumin (BSA), PBS tablets (140 mM NaCl, 10 mM phosphate buffer, 3 mM KCl) (pH 7.4), Potassium hexacyanoferrate(III) ($K_3[Fe(CN)_6]$), Potassium chloride (KCl) and thrombin human plasma were purchased from Merck Life Science (St. Louis, MO, USA). Plasma samples used for spiking experiments were obtained from local clinical laboratories and originated from healthy volunteers. Leptin was purchased by the Department of molecular medicine and medical biotechnology of Federico II University of Naples. All solutions were prepared in Milli-Q water produced in-house to 18 MΩ/cm quality, using a Milli-Q® EQ (7015) Ultrapure Water Purification System (Darmstadt, Germany). Conductive inks (Ag/AgCl and graphite) were purchased from Sun Chemicals (USA). Flexible polyester film (HT5 Autostat) was kindly provided by McDermid Alpha (UK) and MacDermid Performance Solutions Italiana (Italy). For the fabrication of the paper-based preconcentration device commercial filter paper (CFP), intended for general use such as bench protection with a thickness of 135 μm, was obtained from MyCordenons (Milano, Italy).

2.2. Screen-printed electrodes preparation

Electrodes were in-house produced onto a flexible polyester film as substrate. The three-electrode design was screen-printed using a semi-automatic screen-printer equipped with a squeegee to spread the conductive inks through an ad-hoc designed mask. Briefly, Ag/AgCl ink was used to print the connections and the reference electrode, and the carbon ink was used to print the working and counter electrodes. After the inks were printed, the strips were thermally cured, 100 °C for 30 min, necessary to make the printed ink stable for electrochemical measurements. The diameter of the working electrode was 0.4 cm, and the electrochemical strips were ca. 2.5 cm (height) x 1 cm (width). The possible diffusion of aqueous samples to the connector was avoided by placing an adhesive tape to define the testing area (Miglione et al., 2022a, 2022b).

2.3. Electrochemical measurements

All the electrochemical measurements were carried out using a portable potentiostat PalmSens 4 (PalmSens, Netherlands) equipped with a multi-12 reader and interfaced to a laptop using PSTrace5.10. Electrochemical characterization was performed by using cyclic voltammetry (CV) and electrochemical impedance spectroscopy (EIS) in the presence of an external redox couple, namely potassium ferrocyanide and potassium ferricyanide ($[Fe(CN)_6]^{3-/4-}$) prepared in 0.1 M KCl at 1 mM concentration(Cinti et al., 2024). CV was performed in a range between −0.7 and 0.7 V with a scan rate of 0.05 V/s while EIS was performed using a frequency range from 10^{-1}–10^5 Hz with an amplitude perturbation of 5 mV (Carneiro et al., 2017). Aβ(1–42) was detected by using differential pulse voltammetry (DPV) in the range between −0.2 and 0.7 V, with a scan rate of 0.1 V/s. Statistical analyses were carried out using two-tailed Student's *t*-tests (Welch's correction for unequal variances) on replicate datasets (n = 4) in a Python environment run on Google Colab (SciPy library). Differences were considered significant at $p < 0.05$.

2.4. Preparation of the immunosensor

The immunosensors were prepared through a multi-step surface modification procedure, starting with the electrochemical deposition of gold. A 5 mM $HAuCl_4$ solution was electrodeposited onto the working electrode surfaces by applying a potential of −0.2 V for 240 s. Following this, self-assembled monolayers (SAMs) were formed by incubating the electrodes with 10 μL of 0.5 mM MPA (Au/MPA), prepared in water, for 45 min at 25 °C (Carneiro et al., 2017). The electrodes were then washed with deionized water and allowed to dry. To activate the carboxyl groups of the SAMs for covalent binding, 10 μL of a freshly prepared solution of EDC (0.2 M) and NHS (0.1 M) in water was applied to the surfaces and incubated for 15 min at 25 °C. After washing with PBS containing 0.05 % Tween-20, the sensors were allowed to dry. Then, 10 μL of a monoclonal anti-Aβ(1–42) solution (1 μg/mL) was immobilized by incubation for 1 h at 25 °C (Au/MPA/anti-Aβ(1–42)). The electrodes were then gently washed again with PBS-Tween and allowed to dry. To block non-specific binding sites, the surfaces were treated with 1 % BSA for 15 min at 25 °C, followed by a PBS wash and drying (Au/MPA/anti-Aβ(1–42)/BSA) (Fig. 1). All incubation steps were performed in a humid chamber (Carneiro et al., 2017; Lien et al., 2015; Y. Abbasi et al., 2021).

2.5. Electrochemical detection of Aβ(1–42)

Subsequently, the Au/MPA/anti-Aβ(1–42)/BSA electrode was incubated with 10 μL of Aβ(1–42) solution in the range from 0.002 to 10 μg/mL for 30 min at 25 °C and finally rinsed with PBS. All measurements were carried out in quadruplicate (n = 4). DPV experiments were performed in the presence of 70 μL of 1 mM $[Fe(CN)_6]^{3-/4-}$ on top of the strip. Briefly, when Aβ(1–42) is recognized by the immobilized antibody, the diffusion of ferro/ferricyanide towards the electrode area is hindered, resulting in a lower current signal with respect to the signal obtained in absence of the protein (blank). The signal change (% SC) was calculated as:

$$\%\ SC = \frac{I0 - IA\beta(1-42)}{I0} * 100 \quad (1)$$

where I_0 and $I_{A\beta(1-42)}$ are the peak currents of 1 mM $Fe(CN)_6^{3-/4-}$ before and after the incubation with Aβ(1–42), respectively.

2.6. Preconcentration using paper-based origami device

The paper-based origami preconcentration device was fabricated following the procedure reported by Kalligosfyri et al. (Kalligosfyri and Cinti, 2024). Briefly, the circular pattern was designed using Adobe Illustrator and wax-printed onto common filter paper (CFP) using a ColorQube 8880 solid ink wax printer. To create hydrophobic barriers, the wax-printed paper was heated at 100 °C for approximately 1 min. The final device consisted of ten layers: nine layers composed of 3-mm diameter discs, and one bottom layer, where the preconcentration occurs, with a 9-mm diameter disc. For preconcentration, a 10 μL aliquot of sample (prepared in buffer or spiked in undiluted plasma) was applied to each of the ten discs and allowed to dry at room temperature. After drying, the device was folded into its origami configuration, and 10 μL of buffer was added to the top to elute the concentrated analyte into the final collection layer. Once dried, this last layer was carefully cut and the preconcentrated target was reconstituted in 30 μL water for both buffer experiments and undiluted plasma samples (Fig. 1). Subsequently, 10 μL of the preconcentrated solution was incubated on the modified electrode (Au/MPA/anti-Aβ(1–42)/BSA) for 30 min at 25 °C in a humid chamber. After incubation, the electrodes were washed with PBS and the electrochemical measurements were carried out as described above.

The effectiveness of the preconcentration step was evaluated calculating the fold-change and the signal increase (%), respectively as (SC: signal change):

$$Fold\ Change = \frac{\%\ SC\ non\ preconc.}{\%\ SC\ preconc.} \quad (2)$$

$$Signal\ Increase\ (\%) = \frac{\%\ SC\ preconc. - \%\ SC\ non\ preconc.}{\%\ SC\ non\ preconc.} * 100 \quad (3)$$

3. Results and discussion

3.1. Optimization of the immunosensor

The stepwise assembly of the immunoplatform was electrochemically characterized using CV and EIS, as reported in the Supplementary material (Fig. S1 and Fig. S2, respectively). CV was used to monitor changes in the redox response of the $[Fe(CN)_6]^{3-/4-}$ probe during each modification step. After gold electrodeposition, an increased peak current was observed due to the enhanced surface conductivity provided by the freshly deposited nanostructured gold. Upon functionalization with MPA and subsequent biomolecular immobilization steps, a progressive decrease in current was noted. This is attributed to the growing steric hindrance and insulating properties of the molecular layers, which hinder the diffusion of the redox probe to the electrode surface (Fig. S1). Complementarily, EIS provided insight into changes in the interfacial charge transfer resistance (Rct), reflected in the increasing diameter of the Nyquist semicircle after each functionalization step. This increase is

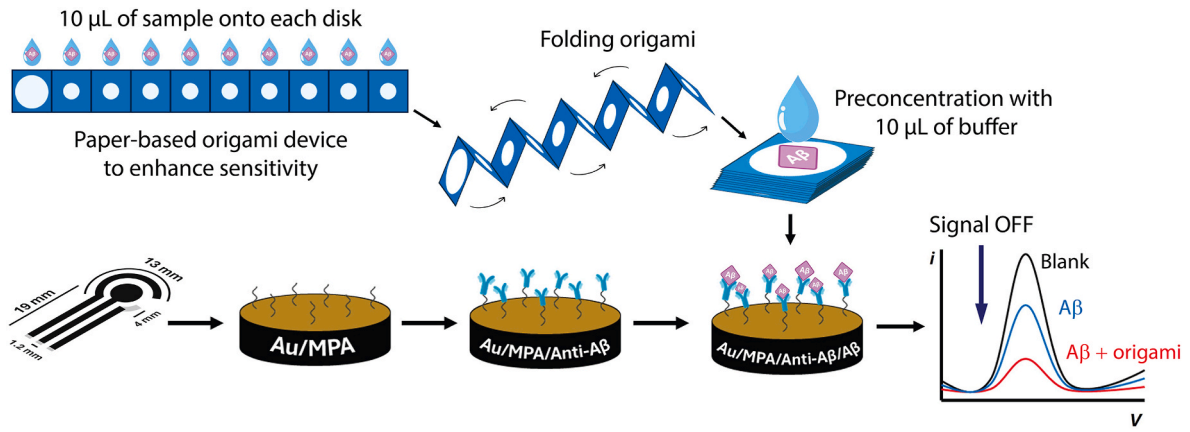

Fig. 1. Schematic illustration of the step-by-step biosensor fabrication and the origami-based preconcentration procedure. Top: sample loading, folding, and elution from the paper-based origami device. Bottom: stepwise modification of the screen-printed electrode with Au, MPA, anti-Aβ, and Aβ(1–42). Right: signal enhancement after preconcentration compared to non-preconcentrated and blank samples.

consistent with the successive assembly of non-conductive layers, first with MPA, then the immobilized antibody, and finally the captured target protein, impeding electron transfer at the electrode interface (Fig. S2) (Lien et al., 2015). Similar trends in *R*ct increase during SAM formation, antibody immobilization, and antigen binding have been widely reported as hallmark signatures of successful biosensor surface assembly (Khare et al., 2022; Ribeiro and Jorge, 2024).

To maximize the biosensor's performance, four key parameters were optimized: the gold nanostructuring method, MPA concentration, antibody concentration, and Aβ(1–42) target incubation time (Fig. 2A, B, 2C and 2D). Electrode surface nanostructuring was first evaluated by comparing two modification strategies: functionalization with gold nanoparticles (AuNPs) by drop-casting (4 μL) and gold electrodeposition (5 mM), in presence of 0.5 μg/mL of Aβ(1–42). As shown in Fig. 2A, electrodeposition resulted in a significantly higher signal change (≈35 %) compared to AuNPs (≈12 %), likely due to better adherence, coverage, and electrical contact of the electrodeposited gold with the underlying carbon surface. A Student's *t*-test confirmed this difference to be highly significant ($p = 0.0002$). This enhancement justified the use of gold electrodeposition in the final sensor fabrication.

The concentration of MPA used to form the self-assembled monolayer (SAM) was next optimized in the range of 0.05–5 mM, in presence of 0.5 μg/mL of Aβ(1–42). As shown in Fig. 2B, the highest signal change was obtained with 0.5 mM MPA. Lower concentrations may lead to incomplete surface coverage, whereas higher concentrations could result in densely packed SAM that hinder antibody immobilization or reduce surface accessibility. Student's t-tests confirmed that 0.5 mM gave a significantly greater signal than 0.05 mM ($p = 0.015$), while the difference with 5 mM was not significant ($p = 0.147$). This supports 0.5 mM as the optimal concentration, balancing efficient coverage with surface accessibility for antibody immobilization (Carneiro et al., 2017).

Consequently, the anti-Aβ(1–42) antibody concentration was varied from 0.01 to 10 μg/mL to determine the optimal surface loading (Fig. 2C). The highest signal change was obtained at 1 μg/mL. This concentration was statistically higher than 0.01 μg/mL ($p = 0.0013$), 0.1 μg/mL ($p = 0.0015$), and 10 μg/mL ($p = 0.0035$), as confirmed by *t*-tests, suggesting effective antibody immobilization with sufficient binding sites for target capture. Higher concentrations did not improve the response, possibly due to steric hindrance or multilayer formation leading to lower antigen accessibility.

Lastly, the incubation time of 0.5 μg/mL Aβ(1–42) target on the immunosensor was optimized by testing three time intervals: 15, 30, and 60 min (Fig. 2D). A 30-min incubation provided the highest signal change, indicating optimal antigen-antibody interaction within this time frame. Student's *t*-tests confirmed that 30 min was significantly higher than both 15 min ($p = 0.0016$) and 60 min ($p = 0.000005$). Shorter incubation may lead to incomplete binding, while prolonged exposure may result in non-specific interactions or desorption effects. These optimization steps ensured maximal sensitivity of the final immunosensor, enabling efficient and reproducible detection of Aβ(1–42) with minimal non-specific signal.

3.2. Analytical performance

The analytical performance of the developed label-free immunosensor for Aβ(1–42) detection was assessed by differential pulse voltammetry (DPV) in the presence of 1 mM $[Fe(CN)_6]^{3-/4-}$. As illustrated in Fig. 3B, increasing concentrations of Aβ(1–42) caused a progressive decrease in current signal, consistent with hindered diffusion of the redox probe due to the formation of the antibody–antigen complex on the electrode surface. The resulting calibration curve (Fig. 3A) was constructed by plotting the percentage signal change versus Aβ(1–42) concentration in the range of 0.005–10 μg/mL, yielding exponential-like response that was fitted using a non-linear regression model. A well-

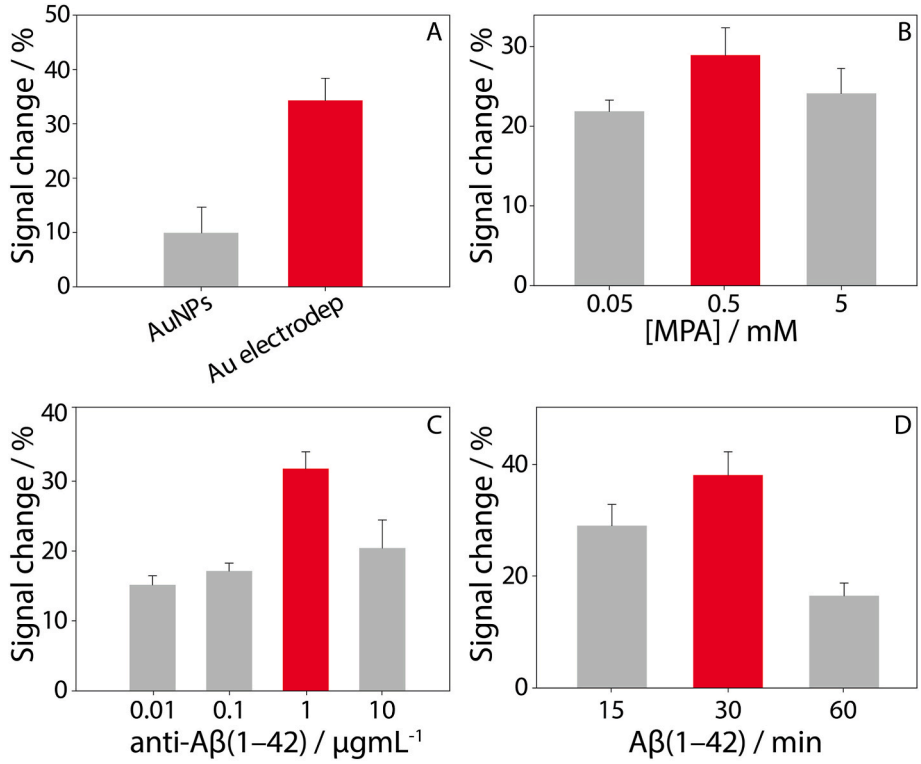

Fig. 2. Optimization of the immunosensor using DPV in the presence of 1 mM $[Fe(CN)_6]^{3-/4-}$ redox probe. A) Comparison between electrode modification using 4 μL of gold nanoparticles (AuNPs) and 5 mM of electrodeposited gold. B) Effect of different concentrations (0.05–5 mM) of MPA on sensor response. C) Optimization of anti-Aβ(1–42) antibody concentration (0.01–10 μg/mL). D) Effect of incubation time with 0.5 μg/mL Aβ(1–42) target (15–60 min). The antibody concentration was fixed at 10 μg/mL for all panels except (C). Significance is indicated as $p < 0.05$ (*), $p < 0.01$ (**), $p < 0.001$ (***) and $p > 0.05$ (ns). Error bars represent standard deviation (n = 4). DPV parameters: E begin = −0.2 V, E end = +0.7 V, E step = 0.01 V, E pulse = 0.2 V, t pulse = 0.02 s, scan rate = 0.1 V/s.

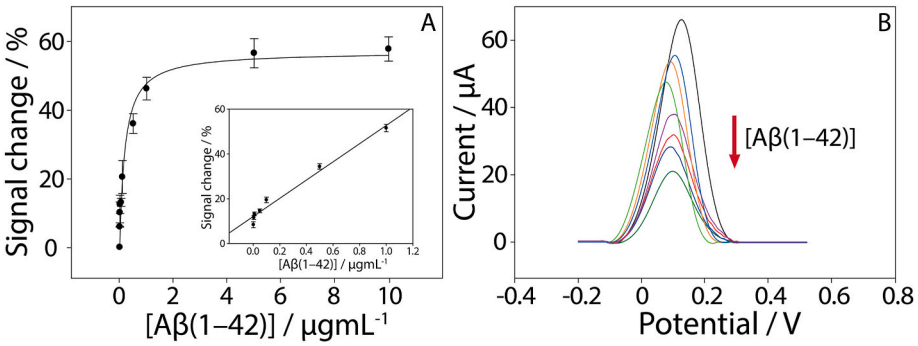

Fig. 3. A) Calibration curve of the label-free immunosensor for Aβ(1–42) detection obtained by DPV in the presence of 1 mM $[Fe(CN)_6]^{3-/4-}$. The response was evaluated as % signal change versus Aβ(1–42) concentration in the range 0–10 μg/mL. Inset: linear range between 0.002 and 1.0 μg/mL. Error bars represent standard deviation (n = 4). B) DPV curves showing the decrease in current intensity with increasing Aβ(1–42) concentrations (0–10 μg/mL), attributed to the hindered diffusion of the redox probe due to antigen–antibody binding on the electrode surface.

defined linear range was observed between 0.002 and 1 μg/mL, described by the linear regression equation: y = 40.4x + 12.2 (R^2 = 0.97), where y is the signal change (%) and x is the Aβ(1–42) concentration (μg/mL). Based on this range, the limit of detection (LOD) and limit of quantification (LOQ) were calculated as 2.7 ng/mL and 9.0 ng/mL, respectively, using the $3\sigma b/m$ and $10\sigma b/m$ criteria (where σb is the standard deviation of the blank signals and m the slope of the regression line). The immunosensor demonstrated excellent repeatability, with a relative standard deviation (RSD%) of 6.0 % (n = 4) for the intermediate concentration of 0.5 μg/mL.

3.3. Selectivity studies

A crucial issue in the development of any biosensor is the selection of highly specific biological receptors for the target. In this respect, the potential interference and cross-reactivity of the capture antibody toward non-target proteins commonly present in biological fluids was evaluated to assess the selectivity of the proposed immunosensor. Selectivity tests were performed by applying the sensor to individual non-target proteins and mixtures containing both the interfering protein and the target Aβ(1–42). The chosen interferents included leptin (0.1 μg/mL) (Chu et al., 2001), human plasma thrombin (0.1 μg/mL) (Iannucci et al., 2020), and bovine serum albumin (BSA) (1 mg/mL). These proteins were selected based on their abundance or relevance in plasma and their molecular size, which is comparable to or greater than that of Aβ(1–42). Leptin is a low molecular weight cytokine-like hormone (~16 kDa) with potential structural similarity to peptide biomarkers, thrombin is a ~37 kDa serine protease involved in coagulation and often present during inflammatory states, including those observed in neurodegenerative conditions (Iannucci et al., 2020). BSA is not naturally present in human plasma, but it was included in the selectivity study due to its structural similarity to human serum albumin and its common use in biosensor systems as a blocking agent. Its high concentration (1 mg/mL) also serves as a worst-case scenario to evaluate potential non-specific adsorption effects.

As shown in Fig. 4, the immunosensor exhibited negligible signal changes (up to 4 %), when exposed to these proteins individually, confirming the high specificity of the anti-Aβ(1–42) antibody. Moreover, when each interferent was tested in combination with 0.1 μg/mL of Aβ (1–42), the sensor response was consistent with the Aβ(1–42)-only control, with no significant deviations observed. Student's t-tests were performed to compare sensor responses under different selectivity conditions. While leptin (p = 0.027) and BSA (p = 0.009) alone showed statistically significant deviations from the blank, all interferent + Aβ mixtures showed no significant difference compared to the Aβ-only condition (p > 0.05). This indicates that the presence of non-specific plasma proteins does not hinder the ability of the biosensor to accurately recognize and respond to its target.

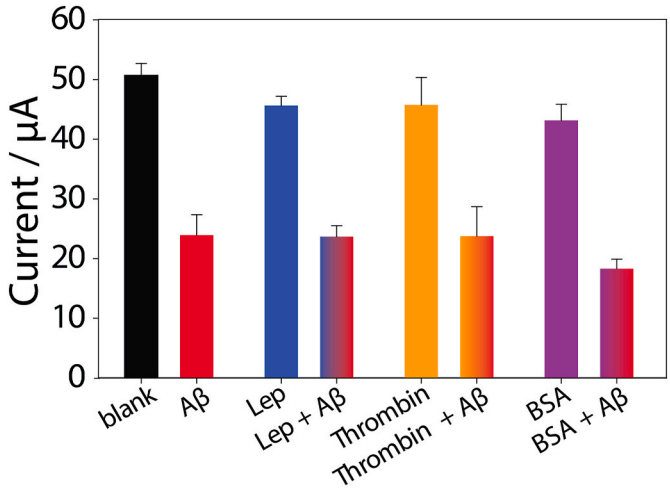

Fig. 4. Selectivity assessment of the developed immunosensor against non-target proteins. Current responses were recorded after incubation with: blank (PBS only), Aβ(1–42) (0.1 μg/mL), leptin (Lep, 0.1 μg/mL), thrombin human plasma (0.1 μg/mL), and bovine serum albumin (BSA, 1 mg/mL), both alone and in combination with Aβ(1–42). Significance is indicated as $p < 0.05$ (*) and $p < 0.01$ (**); all interferent + Aβ mixtures were not significantly different from Aβ alone ($p > 0.05$). Measurements performed in the presence of 1 mM $[Fe(CN)_6]^{3-/4-}$. Error bars represent standard deviation (n = 4).

3.4. Application in spiked healthy plasma samples

To assess the practical applicability of the developed immunosensor in clinically relevant matrices, its performance was evaluated using undiluted human plasma samples spiked with known concentrations of Aβ(1–42). Measurements were carried out under the same conditions as those used in buffer, using DPV in the presence of 1 mM $[Fe(CN)_6]^{3-/4-}$. As shown in Fig. 5A, the calibration curve obtained in plasma followed an exponential-like trend similar to that observed in buffer. A linear response was retained in the concentration range of 0–0.1 μg/mL, described by the linear regression equation: y = 293.6x + 2.0 (R^2 = 0.98), achieving a LOD of 4.7 ng/mL and a LOQ of 15.7 ng/mL. Interestingly, the linear range in undiluted plasma was narrower compared to that observed in buffer. This reduction may be attributed to matrix effects arising from the complex composition of plasma, such as proteins, lipids, and other interfering substances. These components can partially foul the electrode surface or compete for surface binding sites, potentially reducing the accessibility of the immobilized antibodies, and leading to earlier signal saturation. The corresponding DPV profiles (Fig. 5B) exhibited a consistent decrease in current signal with

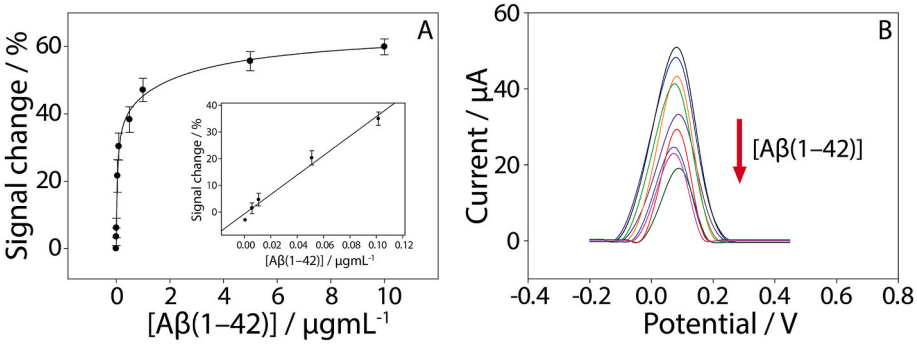

Fig. 5. A) Calibration curve of the electrochemical immunosensor in undiluted human plasma spiked with increasing concentration of Aβ(1–42), in the range from 0 to 10 μg/mL range. Inset: linear range from 0 to 0.1 μg/mL. Error bars represent standard deviation (n = 4). B) Corresponding DPV curves in the presence of 1 mM $[Fe(CN)_6]^{3-/4-}$, showing a progressive decrease in current with increasing β-amyloid concentrations.

increasing Aβ(1–42) concentration, confirming that the sensor remained responsive in the complex plasma matrix without requiring dilution or pretreatment.

These findings demonstrate that the sensor is capable of performing direct, label-free detection of Aβ(1–42) in undiluted plasma, a key step toward real-world application in point-of-care Alzheimer's diagnostics.

3.5. Preconcentration strategy using an origami paper-based device

While the developed label-free immunosensor exhibited good sensitivity, with limits of detection of 2.7 ng/mL in buffer and 4.7 ng/mL in plasma, these values are still above the sub-ng/mL concentrations typically reported for circulating Aβ(1–42) in early-stage Alzheimer's disease (Chen et al., 2019; Lue et al., 2017; Zecca et al., 2018). To overcome this limitation and enhance the detection capability of the platform, we employed a paper-based origami preconcentration device, previously developed by our group for nucleic acid enrichment (Glovi et al., 2025), without external instrumentation. This approach utilizes a 10-layer folded device made from commercial filter paper, enabling passive capillary-driven enrichment of the target within 1 min. The procedure and device configuration are described in detail in the Experimental Section. The origami device was applied for the preconcentration of Aβ(1–42) at low concentrations (0.005, 0.01, and 0.05 μg/mL) in both buffer and undiluted plasma. In buffer, as shown in Fig. 6A and B, the signal change increased after preconcentration, with fold-change values of 4x to 5x, corresponding to a signal increase of 316–394 % across all tested concentrations. Student's t-tests confirmed that the increases were highly significant at all concentrations (p =

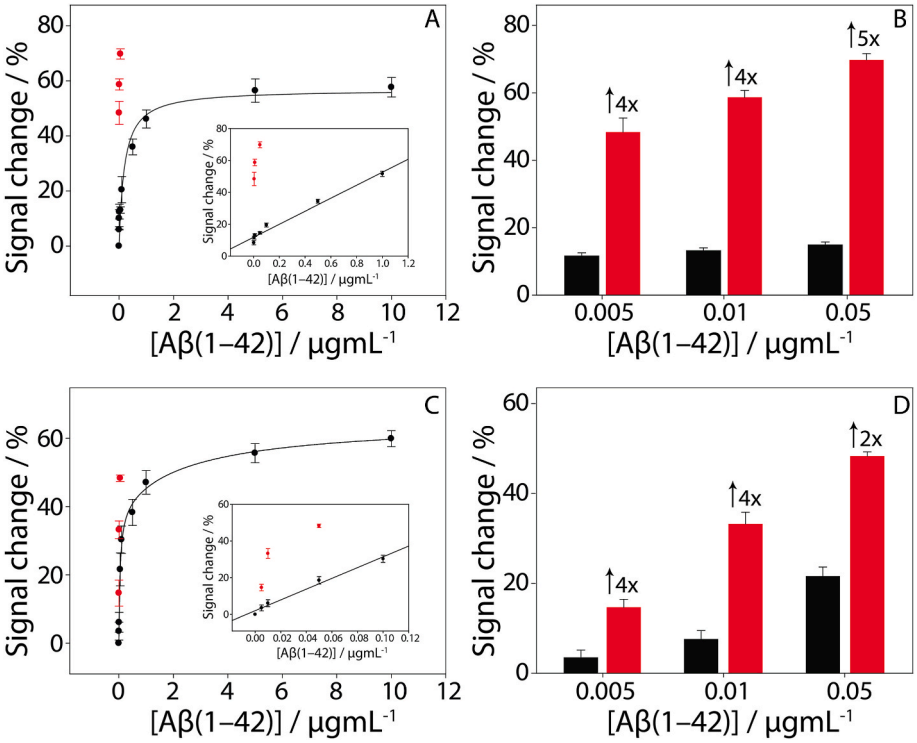

Fig. 6. A) Calibration curve of the immunosensor for Aβ(1–42) in buffer (black), overlaid with the signal after origami preconcentration of samples at 0.005, 0.01, and 0.05 μg/mL (red). Inset: Inset: zoom on the linear region used for comparison. (B) Corresponding signal change (%) with (red) and without preconcentration (black) in buffer. C) Calibration curve of the immunosensor for Aβ(1–42) in undiluted plasma (black), overlaid with the signal after origami preconcentration of samples at 0.005, 0.01, and 0.05 μg/mL (red). Inset: zoom on the linear region used for comparison. D) Corresponding signal change (%) with (red) and without preconcentration (black) in plasma. Fold-increases (2x–5x) are indicated. Student's *t*-tests confirmed that preconcentration significantly increased the response at all concentrations in both buffer and plasma; significance is indicated as $p < 0.05$ (*), $p < 0.01$ (**), *and* $p < 0.001$ (***). Error bars represent standard deviation (n = 4).

0.0036 to 0.000006). This confirms the effectiveness of the paper-based enrichment system in improving the current signal of the target analyte.

In plasma, the effect was still substantial but somewhat attenuated. As reported in Fig. 6C and D, a 4x signal enhancement was obtained at the two lower concentrations (0.005 and 0.01 μg/mL), while only a 2x increase was observed at 0.05 μg/mL. All improvements were statistically significant ($p = 0.032$ to 0.0088), confirming that the preconcentration strategy remains effective even in complex biological matrices. The reduced amplification may be attributed to the earlier onset of signal saturation in plasma, as also observed in the non-preconcentrated calibration curve (Fig. 5A), where the plateau region is reached at lower concentrations compared to buffer (Fig. 3A). This behavior likely reflects matrix-related effects, such as the presence of abundant plasma proteins, which can contribute to biofouling, compete for surface interactions, or limit antigen diffusion toward the immobilized antibody. Despite this limitation at higher concentrations, the origami device significantly enhanced detection sensitivity at lower clinically relevant levels, confirming its utility for real-world applications.

To contextualize our platform, Table 1 summarizes representative electrochemical Aβ(1–42) biosensors spanning label-free impedimetric/voltammetric formats and recent micro/nanostructured or micromotor-assisted assays. While several state-of-the-art devices achieve very low LODs (often in the pg/mL range), they frequently rely on complex nanostructures, sandwich formats, or auxiliary actuation, which may limit scalability or practical deployment. In contrast, our design is based on screen-printed electrodes and a simple, equipment-free paper origami module, emphasizing manufacturability, low cost, and operational simplicity alongside competitive sensitivity.

Despite the extremely low concentrations of Aβ(1–42) in plasma, typically in the 10–50 pg/mL range, which remain challenging to detect using label-free strategies, the proposed platform marks a significant advancement toward accessible and decentralized Alzheimer's diagnostics. While our current LOD remains in the low ng/mL range, the integration with a origami-based preconcentration step enabled sensitive detection of Aβ(1–42) at concentrations approaching clinical relevance. At the lowest tested concentrations, this approach provided ~4-fold signal enhancement in both buffer and plasma, which is expected to proportionally reduce the effective LOD, although a formal recalculation was not performed in the absence of a dedicated calibration. Our system combines scalable materials, minimal sample processing, and label-free electrochemical detection, laying the groundwork for future development of affordable, portable tools that could extend Alzheimer's screening to resource-limited or point-of-care settings.

4. Conclusions

A label-free electrochemical immunosensor based on a screen-printed electrode for the sensitive detection of β-amyloid (Aβ(1–42)) was developed exploiting a paper-based origami device to improve the analytical performance of the ultimate device. The immunoplatform was thoroughly optimized in terms of surface modification, antibody loading, and assay conditions to achieve reproducible and selective recognition of the target protein. The sensor demonstrated good analytical performance, with limits of detection of 2.7 ng/mL in buffer and 4.7 ng/mL in undiluted plasma, and high selectivity against common plasma proteins such as leptin, thrombin, and BSA. However, considering that Aβ(1–42) levels in plasma can fall below 1 ng/mL in early-stage Alzheimer's, we implemented a paper-based origami preconcentration strategy to enhance detection sensitivity. This approach enabled rapid, equipment-free enrichment of Aβ(1–42) and resulted in a sensitivity enhancement of up to 5-fold, demonstrating this procedure particularly effective for the detection of low concentrations of the chosen target. Overall, the proposed immunosensor, when combined with the origami preconcentration step, represents a promising and scalable tool for point-of-care screening and longitudinal monitoring of Alzheimer's disease. Its simplicity, label-free design, and compatibility with low-cost materials make it suitable for future integration into portable diagnostic platforms targeting neurodegenerative diseases.

CRediT authorship contribution statement

Antonella Miglione: Writing – review & editing, Writing – original draft, Methodology, Investigation, Formal analysis, Data curation, Conceptualization. **Panagiota M. Kalligosfyri:** Writing – review & editing, Methodology, Data curation, Conceptualization. **Claudia Corbo:** Visualization, Resources, Funding acquisition. **Donato Calabria:** Visualization, Resources, Funding acquisition. **Mara Mirasoli:** Visualization, Resources, Funding acquisition. **Marco Frasconi:** Visualization, Resources, Funding acquisition. **Stefano Cinti:** Writing – review & editing, Visualization, Resources, Funding acquisition, Conceptualization.

Table 1
Comparison of representative electrochemical biosensors reported for Aβ(1–42) detection.

Platform	Technique	Linear range	LOD (ng/mL)	Application	Ref.
Competitive immunosensor on Au-nanostructured SPCE	CV	0.5–500 ng/mL	0.1 ng/mL	Buffer	Rama et al. (2014)
Label-free immunosensor on carbon DEP chip	EIS	0.045–451 ng/mL	2.6 ng/mL	Buffer	Lien et al. (2015)
Polycrystalline gold label-free immunosensor cell	SWV	10–1000 pg/mL	0.005 ng/mL	Buffer	Carneiro et al. (2017)
Polycrystalline microporous Au nanostructure	DPV	0.003–7 ng/mL	0.0002 ng/mL	Diluted serum and artificial CSF	Negahdary and Heli (2019)
Graphene/rGO dual-layer label-free SPE	DPV	0.050–248 ng/mL	0.01 ng/mL	Spiked human and mice plasmas	Sethi et al. (2020)
Label-free SPGE modified with pDAN	DPV	0.001 ng/mL - 1 ng/mL	0.0014 ng/mL	Spiked diluted human plasma	(Y. Abbasi et al., 2021)
Superwettable substrate based on VG@Au	DPV	0.0001–1 ng/mL	0.000012 ng/mL	Diluted goat serum	Huang et al. (2022)
PPy/Ni/PtNPs MM SPCE	Amperometry	0.2–50 ng/mL	0.06 ng/mL	Brain tissue, CSF and plasma samples	Gordón Pidal et al. (2024)
Paper-based origami SPE	DPV	2–1000 ng/mL in buffer 0–100 ng/mL in serum	2.7 ng/mL in buffer and 4.7 ng/mL in plasma*	Spiked undiluted plasma	This work

SPCE/SPGE: Screen-printed carbon/graphene electrodes; CV: Cyclic voltammetry; DEP: disposable electrochemical printed; EIS: electrochemical impedance spectroscopy; SWV: Square-wave voltammetry; DPV: Differential pulse voltammetry; CSF: cerebrospinal fluid; pDAN: polymerised 1,5-diaminonaphthalene; VG@Au: nanoAu-modified vertical graphene; PPy/Ni/PtNPs MM: polypyrrole/nickel/platinum nanoparticles micromotor; *Origami preconcentration provided ~4 × signal enhancement at the lowest concentrations in buffer and plasma (Fig. 6). A formal LOD for the preconcentration workflow was not established.

Declaration of competing interest

The authors declare that they have no known competing financial interests or personal relationships that could have appeared to influence the work reported in this paper.

Acknowledgements

A.M and S.C. PRIN project No. 2022WN89PC entitled “Biomimetic sensing platforms for the detection of Alzheimer’s disease related biomarkers” is acknowledged.

S.C. acknowledges the Pathogen Readiness Platform for CERIC-ERIC Upgrade” PRP@CERIC è finanziato dal PNRR Piano Nazionale di Ripresa e Resilienza nell’ambito della Missione 4 “Istruzione e Ricerca,” Componente 2 “Dalla Ricerca all’Impresa”, Linea di Investimento 3.1 “Fondo per la realizzazione di un sistema inte-grato di infrastrutture di ricerca e innovazione”, finanziato dall’Unione Europea—Next Generation EU.

P.M. Kalligosfyri acknowledges Fondazione Umberto Veronesi Postdoctoral Fellowship 2025.

MacDermid Alpha - Film & Smart Surface Solutions is acknowledged for providing the polyester sheets Autostat HT5.

Appendix A. Supplementary data

Supplementary data to this article can be found online at https://doi.org/10.1016/j.biosx.2025.100687.

Data availability

Data will be made available on request.

References

Azargoonjahromi, A., 2024. The duality of amyloid-β: its role in normal and Alzheimer’s disease states. Mol. Brain 17, 44. https://doi.org/10.1186/s13041-024-01118-1.

Bellomo, G., Bayoumy, S., Megaro, A., Toja, A., Nardi, G., Gaetani, L., Blujdea, E.R., Paolini Paoletti, F., Wojdała, A.L., Chiasserini, D., van der Flier, W.M., Verberk, I.M. W., Teunissen, C., Parnetti, L., 2024. Fully automated measurement of plasma Aβ42/40 and p-tau181: analytical robustness and concordance with cerebrospinal fluid profile along the Alzheimer’s disease continuum in two independent cohorts. Alzheimer’s Dementia 20, 2453–2468. https://doi.org/10.1002/alz.13687.

Bouwman, F.H., Frisoni, G.B., Johnson, S.C., Chen, X., Engelborghs, S., Ikeuchi, T., Paquet, C., Ritchie, C., Bozeat, S., Quevenco, F.-C., Teunissen, C., 2022. Clinical application of CSF biomarkers for Alzheimer’s disease: from rationale to ratios. Alzheimer’s Dementia: Diagnosis, Assessment & Disease Monitoring 14, e12314. https://doi.org/10.1002/dad2.12314.

Bun, S., Ito, D., Tezuka, T., Kubota, M., Ueda, R., Takahata, K., Moriguchi, S., Kurose, S., Momota, Y., Suzuki, N., Morimoto, A., Hoshino, Y., Seki, M., Mimura, Y., Shikimoto, R., Yamamoto, Y., Hoshino, T., Sato, Y., Tabuchi, H., Mimura, M., 2023. Performance of plasma Aβ42/40, measured using a fully automated immunoassay, across a broad patient population in identifying amyloid status. Alzheimers Res. Ther. 15, 149. https://doi.org/10.1186/s13195-023-01296-5.

Carneiro, P., Loureiro, J., Delerue-Matos, C., Morais, S., do Carmo Pereira, M., 2017. Alzheimer’s disease: development of a sensitive label-free electrochemical immunosensor for detection of amyloid beta peptide. Sensor. Actuator. B Chem. 239, 157–165. https://doi.org/10.1016/j.snb.2016.07.181.

Chen, T.-B., Lee, Y.-J., Lin, S.-Y., Chen, J.-P., Hu, C.-J., Wang, P.-N., Cheng, I.H., 2019. Plasma Aβ42 and total tau predict cognitive decline in amnestic mild cognitive impairment. Sci. Rep. 9, 13984. https://doi.org/10.1038/s41598-019-50315-9.

Chiorcea-Paquim, A.-M., Oliveira-Brett, A.M., 2022. Amyloid beta peptides electrochemistry: a review. Curr. Opin. Electrochem. 31, 100837. https://doi.org/10.1016/j.coelec.2021.100837.

Chu, N.F., Stampfer, M.J., Spiegelman, D., Rifai, N., Hotamisligil, G.S., Rimm, E.B., 2001. Dietary and lifestyle factors in relation to plasma leptin concentrations among normal weight and overweight men. Int. J. Obes. 25, 106–114. https://doi.org/10.1038/sj.ijo.0801468.

Cimmino, W., Raucci, A., Grosso, S.P., Normanno, N., Cinti, S., 2024. Enhancing sensitivity towards electrochemical miRNA detection using an affordable paper-based strategy. Anal. Bioanal. Chem. 416, 4227–4236. https://doi.org/10.1007/s00216-024-05406-6.

Cinti, S., Tomassi, S., Ciardiello, C., Migliorino, R., Pirozzi, M., Leone, A., Di Gennaro, E., Campani, V., De Rosa, G., D’Amore, V.M., Di Maro, S., Donati, G., Singh, S., Raucci, A., Di Leva, F.S., Kessler, H., Budillon, A., Marinelli, L., 2024. Paper-based electrochemical device for early detection of integrin αvβ6 expressing tumors. Commun. Chem. 7, 1–9. https://doi.org/10.1038/s42004-024-01144-z.

Delaby, C., Hirtz, C., Lehmann, S., 2023. Overview of the blood biomarkers in Alzheimer’s disease: promises and challenges. Rev. Neurol. 179, 161–172. https://doi.org/10.1016/j.neurol.2022.09.003.

Ding, M., Ding, S., Du, D., Wang, X., Hu, X., Guan, P., Lyu, Z., Lin, Y., 2023. Recent advances in electrochemical biosensors for the detection of Aβ42, a biomarker for Alzheimer disease diagnosis. TrAC, Trends Anal. Chem. 164, 117087. https://doi.org/10.1016/j.trac.2023.117087.

Glovi, A., Kalligosfyri, P.M., Miglione, A., Singh, S., Iula, G., Giordano, A., De Laurentiis, M., Cinti, S., 2025. Towards liquid biopsy on chip for triple negative breast cancer: preliminary results on monitoring circulating miRNA-21 using portable diagnostics. Discov. Oncol. 16, 1022. https://doi.org/10.1007/s12672-025-02846-z.

Gordón Pidal, J.M., Moreno-Guzmán, M., Montero-Calle, A., Valverde, A., Pingarrón, J. M., Campuzano, S., Calero, M., Barderas, R., López, M.Á., Escarpa, A., 2024. Micromotor-based electrochemical immunoassays for reliable determination of amyloid-β (1–42) in Alzheimer’s diagnosed clinical samples. Biosens. Bioelectron. 249, 115988. https://doi.org/10.1016/j.bios.2023.115988.

Hassan, Q., Kerman, K., 2019. Electrochemical approaches for the detection of amyloid-β, tau, and α-synuclein. Curr. Opin. Electrochem. 14, 89–95. https://doi.org/10.1016/j.coelec.2018.12.009.

Huang, Z., Li, M., Zhang, L., Liu, Y., 2022. Electrochemical immunosensor based on superwettable microdroplet array for detecting multiple Alzheimer’s disease biomarkers. Front. Bioeng. Biotechnol. 10, 1029428. https://doi.org/10.3389/fbioe.2022.1029428.

Iannucci, J., Renehan, W., Grammas, P., 2020. Thrombin, a mediator of coagulation, inflammation, and neurotoxicity at the neurovascular interface: implications for alzheimer’s disease. Front. Neurosci. 14, 762. https://doi.org/10.3389/fnins.2020.00762.

Janelidze, S., Stomrud, E., Palmqvist, S., Zetterberg, H., van Westen, D., Jeromin, A., Song, L., Hanlon, D., Tan Hehir, C.A., Baker, D., Blennow, K., Hansson, O., 2016. Plasma β-amyloid in Alzheimer’s disease and vascular disease. Sci. Rep. 6, 26801. https://doi.org/10.1038/srep26801.

Kalligosfyri, P.M., Cinti, S., 2024. 3D paper-based origami device for programmable multifold analyte preconcentration. Anal. Chem. 96, 9773–9779. https://doi.org/10.1021/acs.analchem.4c02032.

Karapetyan, G., Fereshetyan, K., Harutyunyan, H., Yenkoyan, K., 2022. The synergy of β amyloid 1-42 and oxidative stress in the development of Alzheimer’s disease-like neurodegeneration of hippocampal cells. Sci. Rep. 12, 17883. https://doi.org/10.1038/s41598-022-22761-5.

Karran, E., De Strooper, B., 2022. The amyloid hypothesis in alzheimer disease: new insights from new therapeutics. Nat. Rev. Drug Discov. 21, 306–318. https://doi.org/10.1038/s41573-022-00391-w.

Khare, R., Verma, S., Singh, P., Pal, S., Shrivastava, R., 2022. Blueprint for impedance-based electrochemical biosensors as bioengineered tools in the field of nano-diagnostics. Curr. Res. Biotechnol. 4, 564–578. https://doi.org/10.1016/j.crbiot.2022.11.001.

Kirmess, K.M., Meyer, M.R., Holubasch, M.S., Knapik, S.S., Hu, Y., Jackson, E.N., Harpstrite, S.E., Verghese, P.B., West, T., Fogelman, I., Braunstein, J.B., Yarasheski, K.E., Contois, J.H., 2021. The PrecivityAD™ test: accurate and reliable LC-MS/MS assays for quantifying plasma amyloid beta 40 and 42 and apolipoprotein E proteotype for the assessment of brain amyloidosis. Clin. Chim. Acta 519, 267–275. https://doi.org/10.1016/j.cca.2021.05.011.

Knopman, D.S., Amieva, H., Petersen, R.C., Chételat, G., Holtzman, D.M., Hyman, B.T., Nixon, R.A., Jones, D.T., 2021. Alzheimer disease. Nat. Rev. Dis. Primers 7, 33. https://doi.org/10.1038/s41572-021-00269-y.

Korecka, M., Shaw, L.M., 2021. Mass spectrometry-based methods for robust measurement of Alzheimer’s disease biomarkers in biological fluids. J. Neurochem. 159, 211–233. https://doi.org/10.1111/jnc.15465.

Li, M., Zeng, Y., Huang, Z., Zhang, L., Liu, Y., 2023. Vertical graphene-based printed electrochemical biosensor for simultaneous detection of four Alzheimer’s disease blood biomarkers. Biosensors 13, 758. https://doi.org/10.3390/bios13080758.

Lien, T.T.N., Takamura, Y., Tamiya, E., Vestergaard, M.C., 2015. Modified screen printed electrode for development of a highly sensitive label-free impedimetric immunosensor to detect amyloid beta peptides. Anal. Chim. Acta 892, 69–76. https://doi.org/10.1016/j.aca.2015.08.036.

Lue, L.-F., Sabbagh, M.N., Chiu, M.-J., Jing, N., Snyder, N.L., Schmitz, C., Guerra, A., Belden, C.M., Chen, T.-F., Yang, C.-C., Yang, S.-Y., Walker, D.G., Chen, K., Reiman, E. M., 2017. Plasma levels of Aβ42 and Tau identified probable Alzheimer’s dementia: findings in two cohorts. Front. Aging Neurosci. 9, 226. https://doi.org/10.3389/fnagi.2017.00226.

Mei, C., Zhan, J., Zhu, S., Zhang, Y., Xiong, C., Wang, J., Xu, Y.J., Zhong, H., Cheng, J., 2024. Advances of therapy for Alzheimer’s disease: an updated review. Brain-X 2, e68. https://doi.org/10.1002/brx2.68.

Miglione, A., Raucci, A., Amato, J., Marzano, S., Pagano, B., Raia, T., Lucarelli, M., Fuso, A., Cinti, S., 2022a. Printed electrochemical strip for the detection of miRNA-29a: a possible biomarker related to Alzheimer’s disease. Anal. Chem. 94, 15558–15563. https://doi.org/10.1021/acs.analchem.2c03542.

Miglione, A., Spinelli, M., Amoresano, A., Cinti, S., 2022b. Sustainable copper electrochemical stripping onto a paper-based substrate for clinical application. ACS Meas. Au. 2 (2), 177–184. https://doi.org/10.1021/acsmeasuresciau.1c00059.

Minoshima, S., Drzezga, A.E., Barthel, H., Bohnen, N., Djekidel, M., Lewis, D.H., Mathis, C.A., McConathy, J., Nordberg, A., Sabri, O., Seibyl, J.P., Stokes, M.K., Laere, K.V., 2016. SNMMI Procedure Standard/EANM practice guideline for amyloid PET imaging of the brain 1.0. J. Nucl. Med. 57, 1316–1322. https://doi.org/10.2967/jnumed.116.174615.

Negahdary, M., Heli, H., 2019. An electrochemical peptide-based biosensor for the Alzheimer biomarker amyloid-β(1–42) using a microporous gold nanostructure. Microchim. Acta 186, 766. https://doi.org/10.1007/s00604-019-3903-x.

Rama, E.C., González-García, M.B., Costa-García, A., 2014. Competitive electrochemical immunosensor for amyloid-beta 1-42 detection based on gold nanostructurated Screen-printed carbon electrodes. Sensor. Actuator. B Chem. 201, 567–571. https://doi.org/10.1016/j.snb.2014.05.044.

Raucci, A., Sorrentino, G., Singh, S., Borbone, N., Oliviero, G., Piccialli, G., Terracciano, M., Cinti, S., 2025. Cost-effective, user-friendly detection and preconcentration of thrombin on a sustainable paper-based electrochemical platform. Anal. Bioanal. Chem. 417, 1863–1872. https://doi.org/10.1007/s00216-025-05764-9.

Ribeiro, J.A., Jorge, P.A.S., 2024. Applications of electrochemical impedance spectroscopy in disease diagnosis—A review. Sens. Acutators Rep. 8, 100205. https://doi.org/10.1016/j.snr.2024.100205.

Safiri, S., Ghaffari Jolfayi, A., Fazlollahi, A., Morsali, S., Sarkesh, A., Daei Sorkhabi, A., Golabi, B., Aletaha, R., Motlagh Asghari, K., Hamidi, S., Mousavi, S.E., Jamalkhani, S., Karamzad, N., Shamekh, A., Mohammadinasab, R., Sullman, M.J.M., Şahin, F., Kolahi, A.-A., 2024. Alzheimer's disease: a comprehensive review of epidemiology, risk factors, symptoms diagnosis, management, caregiving, advanced treatments and associated challenges. Front. Med. 11, 1474043. https://doi.org/10.3389/fmed.2024.1474043.

Schindler, S.E., Galasko, D., Pereira, A.C., Rabinovici, G.D., Salloway, S., Suárez-Calvet, M., Khachaturian, A.S., Mielke, M.M., Udeh-Momoh, C., Weiss, J., Batrla, R., Bozeat, S., Dwyer, J.R., Holzapfel, D., Jones, D.R., Murray, J.F., Partrick, K.A., Scholler, E., Vradenburg, G., Young, D., Algeciras-Schimnich, A., Aubrecht, J., Braunstein, J.B., Hendrix, J., Hu, Y.H., Mattke, S., Monane, M., Reilly, D., Somers, E., Teunissen, C.E., Shobin, E., Vanderstichele, H., Weiner, M.W., Wilson, D., Hansson, O., 2024. Acceptable performance of blood biomarker tests of amyloid pathology — recommendations from the global CEO initiative on Alzheimer's disease. Nat. Rev. Neurol. 20, 426–439. https://doi.org/10.1038/s41582-024-00977-5.

Seppälä, T.T., Herukka, S.-K., Hänninen, T., Tervo, S., Hallikainen, M., Soininen, H., Pirttilä, T., 2010. Plasma Aβ42 and Aβ40 as markers of cognitive change in follow-up: a prospective, longitudinal, population-based cohort study. J. Neurol. Neurosurg. Psychiatr. 81, 1123–1127. https://doi.org/10.1136/jnnp.2010.205757.

Sethi, J., Van Bulck, M., Suhail, A., Safarzadeh, M., Perez-Castillo, A., Pan, G., 2020. A label-free biosensor based on graphene and reduced graphene oxide dual-layer for electrochemical determination of beta-amyloid biomarkers. Microchim. Acta 187, 288. https://doi.org/10.1007/s00604-020-04267-x.

Sharma, A., Angnes, L., Sattarahmady, N., Negahdary, M., Heli, H., 2023. Electrochemical immunosensors developed for amyloid-beta and tau proteins, leading biomarkers of Alzheimer's disease. Biosensors 13, 742. https://doi.org/10.3390/bios13070742.

Singh, S., Wang, J., Cinti, S., 2022. Review—an overview on recent progress in screen-printed electroanalytical (Bio)Sensors. ECS Sens. Plus 1, 023401. https://doi.org/10.1149/2754-2726/ac70e2.

Suppiah, S., Didier, M.-A., Vinjamuri, S., 2019. The who, when, why, and how of PET amyloid imaging in management of Alzheimer's Disease—review of literature and interesting images. Diagnostics 9, 65. https://doi.org/10.3390/diagnostics9020065.

U.S. Food and Drug Administration (FDA), 2025. FDA Clears First Blood Test Used in Diagnosing Alzheimer's Disease. FDA Press Release. https://www.fda.gov/news-events/press-announcements/fda-clears-first-blood-test-used-diagnosing-alzheimers-disease. (Accessed 6 July 2025).

Valkova, P., Pohanka, M., 2021. Novel trends in electrochemical biosensors for early diagnosis of alzheimer's disease. Int. J. Anal. Chem., 9984876 https://doi.org/10.1155/2021/9984876, 2021.

Wang, B.-Y., Gu, B.-C., Wang, G.-J., Yang, Y.-H., Wu, C.-C., 2022. Detection of Amyloid-β(1–42) aggregation with a nanostructured electrochemical sandwich immunoassay biosensor. Front. Bioeng. Biotechnol. 10, 853947. https://doi.org/10.3389/fbioe.2022.853947.

Weber, D.M., Taylor, S.W., Lagier, R.J., Kim, J.C., Goldman, S.M., Clarke, N.J., Vaillancourt, D.E., Duara, R., McFarland, K.N., Wang, W., Golde, T.E., Racke, M.K., 2024. Clinical utility of plasma Aβ42/40 ratio by LC-MS/MS in Alzheimer's disease assessment. Front. Neurol. 15, 1364658. https://doi.org/10.3389/fneur.2024.1364658.

Y. Abbasi, H., Tehrani, Z., Devadoss, A., Munem Ali, M., Moradi-Bachiller, S., Albani, D., Guy, J., O, 2021. Graphene based electrochemical immunosensor for the ultra-sensitive label free detection of Alzheimer's beta amyloid peptides Aβ(1–42). Nanoscale Adv. 3, 2295–2304. https://doi.org/10.1039/D0NA00801J.

Zecca, C., Tortelli, R., Panza, F., Arcuti, S., Piccininni, M., Capozzo, R., Barulli, M.R., Barone, R., Cardinali, R., Abbrescia, D., Seripa, D., Brescia, V., Logroscino, G., 2018. Plasma β-amyloid1–42 reference values in cognitively normal subjects. J. Neurol. Sci. 391, 120–126. https://doi.org/10.1016/j.jns.2018.06.006.

Zhang, Jifa, Zhang, Y., Wang, J., Xia, Y., Zhang, Jiaxian, Chen, L., 2024. Recent advances in Alzheimer's disease: mechanisms, clinical trials and new drug development strategies. Signal Transduct. Targeted Ther. 9, 211. https://doi.org/10.1038/s41392-024-01911-3.